

## ARTICLES

**Bulk Structure of the (Inverted) Sponge Phase of the Lyotropic Mixture of Sodium Dodecyl Sulfate, 1-Pentanol, Water, and Cyclohexane****M. Magalhães, A. M. Figueiredo Neto,\* and A. C. Tromba***Instituto de Física, Universidade de São Paulo, Caixa Postal 66318, 05315-970, São Paulo, SP, Brazil**Received: November 7, 2003; In Final Form: July 27, 2004*

Different techniques (light transmittance, optical microscopy, X-ray diffraction, small-angle X-ray scattering, viscosity, and electric conductivity) were used to characterize the structure of the sponge ( $L_3$ ) phase in the bulk of the partial isothermal surface of the phase diagram of the sodium dodecyl sulfate (SDS)/1-pentanol ( $C_5$ )/cyclohexane ( $C_6$ )/water mixture, with  $[SDS]/[C_5] = 0.17$  (square brackets represent the percent molar concentration). The results accumulated from the different experimental techniques point toward an *inverted* structure for the  $L_3$  in the concentration range investigated. A water layer of thickness  $\delta$  separates two nonconnected regions in  $C_6$ . This water layer is separated from  $C_6$  by the polar heads of the SDS and OH groups from the  $C_5$  molecules.

**I. Introduction**

Lyotropic liquid crystal is one of the most interesting examples of self-assembled systems. In these materials, under proper temperature and relative concentration conditions, amphiphilic molecules, in the presence of solvents, self-assemble to form aggregates with different topologies depending on the particular phase. Micelles (small anisotropic aggregates), highly anisometric aggregates, and bicontinuous structures are present in the lyotropic polymorphism. The topology of the phase diagrams of these mixtures is very rich, and one of the most interesting phases identified in lyotropics is the *sponge phase* (also labeled  $L_3$ ).<sup>1</sup>

Despite the fundamental physical–chemical interest in understanding the properties of the  $L_3$  phase, there are interesting applications of this phase in pharmacology<sup>2,3</sup> as vehicles of medicine transport.

The sponge phase is optically isotropic, and in the case of a *direct phase structure*, the experimental observations point toward a microstructure where a surfactant bilayer (thickness  $\delta$ ) of multiply connected topology separates two polar solvent domains over macroscopic distances.<sup>1</sup> The random bilayer surface divides space into “inside” and “outside” regions. A symmetric sponge phase has equal amounts of inside and outside regions, and in an asymmetric sponge phase these regions present different amounts. In the case of the *inverted sponge phase structure*,<sup>4</sup> however, to the best of our knowledge, in the literature there is no systematic study of it characterizing its structural parameters along different paths of the phase diagram. By analogy with the direct structure, one should expect that, in the case of an inverted structure, a layer composed by the polar solvent, of multiply connected topology and thickness  $\delta$ , separates two nonpolar solvent domains over macroscopic distances. In contrast to the direct structure, this layer thickness should not be defined by the principal amphiphilic double layer present in the mixture.

Although the sponge phase is optically isotropic, it exhibits flow-induced birefringence.<sup>5</sup> The bilayer presents a saddle-like topology with local principal curvatures of opposite signs. To some extent its structure can be sketched as a melted cubic structure,<sup>6,7</sup> and an important difference between the  $L_3$  and the usual three-dimensional ordered lyotropic cubic phase is the lack of long-range space ordering and periodicity.

Different techniques have been employed to investigate the structure and physical–chemical properties of the (direct)  $L_3$  phase: freeze–fracture electron microscopy, transport properties,<sup>8</sup> X-ray<sup>9</sup> and neutron<sup>5</sup> scattering (SAXS and SANS, respectively) and diffraction techniques, NMR,<sup>7</sup> and light scattering.<sup>10</sup>

A direct sponge phase was observed in both water-rich and oil-rich mixtures, mostly in the vicinity of swollen lamellar phase domains. Some examples of mixtures presenting sponge phases are the following: sodium bis(2-ethylhexyl) sulfosuccinate (AOT)/dodecanol/water;<sup>7</sup> AOT/brine<sup>10</sup>; *n*-dodecylbetain/pentanol/water;<sup>10</sup> cetylpyridinium chloride/hexanol/brine.<sup>10</sup>

The scattering (X-ray and neutron) patterns of the direct sponge phase are analyzed in different ranges of the scattering vector modulus  $H$  ( $=2\pi q$ ). In the small- $H$  range, due to the correlation between pieces of bilayers, the patterns present a broad band associated with a distance  $d$ ,<sup>7,9,11,12</sup> which keeps with the volume fraction of amphiphile ( $\phi$ ) the relation  $H = 2\pi/d = 2\pi\phi/(\gamma_q\delta)$ , where  $\gamma_q$  is a number larger than 1 ( $\sim 1.5$ ).<sup>13</sup> In the high- $H$  range, the patterns present the typical form factor of a flat bilayer and, in mixtures with carbonic chain tails, also show the typical broad band due to the distance between the chains (at about 0.5 nm). In direct sponge phases, the layer thickness was found to be about twice the length of the principal amphiphile. A crossover from the  $1/H^2$  (at  $H < 2\pi/d$ ) to  $1/H^4$  (at  $H > 2\pi/d$ ) behavior, characteristics of the scattering of a flat bilayer with random orientation and a thin interface, respectively, is observed in the scattering curves (scattering intensity versus  $H$ ).

An interesting lyotropic quaternary mixture presenting the L<sub>3</sub> phase is the one composed by sodium dodecyl sulfate (SDS), cyclohexane (C<sub>6</sub>), 1-pentanol (C<sub>5</sub>), and water.<sup>14,16–19</sup> Depending on the temperature and relative concentrations of the different compounds, this mixture presents, besides the L<sub>3</sub> phase, a lamellar phase.<sup>17,18</sup> The sponge phase domain was identified<sup>19</sup> in the partial isothermal surface  $T = 21.5\text{ }^{\circ}\text{C}$ , in an almost linear locus at  $[\text{SDS} + \text{C}_5] \sim 7.5\%$  (where square brackets represent the molar concentration percent,  $M\%$ ), in both water- and C<sub>6</sub>-rich regions of the phase diagram, surrounded by micellar isotropic phase domains. This mixture, in these particular relative concentrations of the different components, is a potential candidate to present the inverted sponge structure. As stressed before, in contrast to the direct sponge phases, where the structures were extensively studied, the bulk structural characteristics of the inverted sponge phase, to the best of our knowledge, have not been investigated in detail and reported.

In this paper we use different techniques (light transmittance, optical microscopy, X-ray diffraction, small-angle X-ray scattering, viscosity, and electric conductivity) to characterize the structure of the inverted sponge phase in the bulk at this partial isothermal surface of the phase diagram of the SDS/1-pentanol/cyclohexane/water, with  $[\text{SDS}]/[\text{C}_5] = 0.17$ .

## II. Experimental Section and Techniques

**A. Mixture.** The lyotropic samples investigated were from the mixture of sodium dodecyl sulfate (SDS), from Sigma; cyclohexane (C<sub>6</sub>), from Aldrich; 1-pentanol (C<sub>5</sub>), from Merck; and water (triply distilled and deionized). The accuracy in the weighting process was  $\pm 0.1\text{ mg}$ . The different components of the mixture were sealed in an assay tube, and it was shaken in a vortex and centrifuged until complete homogenization of the mixture. This process took about 48 h. After that, each mixture was left at rest for 48 h before the characterization procedure with the different techniques. We checked, by means of the different techniques used in this work, that this period was enough to guarantee the complete homogenization and stabilization of the different phases identified in the phase diagram. To ensure this, we repeated some of the measurements performed in all the phases identified 6 months after the first measurement (performed after 48 h of the sample preparation) and the results obtained were within the error bars given in this work.

**B. Light Transmittance.** The light-transmittance experiments were employed to measure the dynamically induced birefringence in a sponge phase sample. The experimental setup is presented in detail in ref 20. In brief, samples were introduced in a Hellma quartz cell (10 mm  $\times$  10 mm  $\times$  45 mm) and sealed to avoid loss of material by evaporation. Inside the cell there was also a stainless steel plate (7 mm  $\times$  7 mm  $\times$  1 mm) which was kept in contact with a vertical side of the cell, at the upper part of it by the action of a permanent magnet placed outside the cell. Initially the plate was kept in the upper part of the cell at rest for about 1 h. After that time, the magnet was removed and the plate fell vertically (due to gravity), introducing a laminar-type shear flow inside the sample and, consequently, a velocity gradient. This gradient induced birefringence that, after the gradient vanished, relaxed to the original (isotropic) state with a typical relaxation time. A probe laser beam (placed in a plane parallel to the biggest plate surface), incident in the sample region near the plate (about 4 mm far from the plate surface), measured the transmittance as a function of time (sample between crossed polarizers).

**C. Optical Microscopy.** The texture observations were made in a Leitz Orthoplan-pol optical microscope. Samples were

encapsulated in a Hellma rectangular glass cell (50 mm  $\times$  2 mm  $\times$  100 mm) or in flat glass capillaries (microslides) 100  $\mu\text{m}$  thick, positioned in a temperature-controlled device (IN-STECH-HSI) with an accuracy of  $0.1\text{ }^{\circ}\text{C}$ . The temperature of the experiments varied between 20 and  $25\text{ }^{\circ}\text{C}$ .

**D. Viscosity Measurements.** A digital cone–plate rheometer (Brookfield, Model LVDV-III, with a CP-51 cone) was used to measure the viscosity ( $\nu$ ) of the samples. The temperature of the samples was kept constant at  $22.1 \pm 0.1\text{ }^{\circ}\text{C}$ , and the speed rotation of the cone was 10 rpm. Samples were placed in a sealed device to avoid evaporation during the experiment.

**E. Electric ac Conductivity Measurements.** The electric ac specific conductivity ( $\sigma$ ) measurements were performed with a PM6303A Automatic RCL Meter (Phillips). Samples were placed inside a sealed homemade circular parallel plate capacitor. The plates and the different electrical contacts were covered with a gold film, and a sinusoidal voltage (frequency of 1 kHz) was applied. The area of the plates was  $S = 1\text{ cm}^2$  and the distance between them was  $L = 1\text{ cm}$ . The temperature of the sample was kept at  $24 \pm 1\text{ }^{\circ}\text{C}$ . The device allows the measurement of the electric resistance ( $R$ ), and  $\sigma$  is obtained assuming (in the limit of low applied voltages) the ohmic characteristic of the resistor:  $\sigma = L/(RS)$ .

**F. X-ray Scattering and Diffraction Experiments.** The small-angle X-ray scattering (SAXS) experiments were performed in the synchrotron of the LNLS (Laboratório Nacional de Luz Sincrotron, Campinas, Brazil) and in the Laboratório de Cristalografia, São Paulo, Brazil. The sample was encapsulated in a cylindrical glass capillary, of 1 mm diameter, placed in a temperature-controlled device which kept the sample temperature at  $22.0 \pm 0.4\text{ }^{\circ}\text{C}$ . The X-ray wavelength ( $\lambda$ ) and sample-to-detector distance used were 0.1608 nm (0.154 nm in São Paulo) and 1038.7 mm (478 mm in São Paulo), respectively. The scattering vector modulus  $q$  is defined as  $q = H/(2\pi) = \{2 \sin(\theta)\}/\lambda$ , where  $2\theta$  is the scattering angle.

A Rigaku X-ray generator (Model 4057A2, 40 kV and 30 mA), with monochromatic radiation ( $\lambda = 0.154\text{ nm}$ ) and pinhole collimator of 0.5 mm diameter, was also employed in the diffraction experiments. Sample holders and the temperature-controlled device were the same as described above. The temperature was fixed at  $25.0 \pm 0.4\text{ }^{\circ}\text{C}$ , and the patterns were registered in a film.

## III. Results and Discussion

As stressed before, the results presented here were observed in samples taken from the lyotropic mixtures 48 h after their preparation and from the same mixtures stored for a period of about 6 months. We verified that the phase boundaries of the partial isothermal do not appreciably change in the temperature range from  $\sim 20.5$  to  $\sim 25.5\text{ }^{\circ}\text{C}$ .

**A. The Phase Diagram.** Figure 1 shows the partial isothermal ( $T = 21.5\text{ }^{\circ}\text{C}$ ) surface of the phase diagram investigated at  $[\text{SDS}]/[\text{C}_5] \approx 0.17$ . Phase frontiers are indicative since it is not the aim of the paper to determine precisely the L<sub>3</sub> neighboring phase loci. Line 1 and line 2 represent the paths of  $[\text{SDS} + \text{C}_5]$  ( $=\phi_m$ , the molar fraction of amphiphile in the mixture) and  $[\text{C}_6]$  about 7.5% and 25.4%, respectively. The present work improves the identification of the surrounding phases around the sponge phase domain with respect to the previous diagram of ref 19.

Although our interest is focused on the L<sub>3</sub> phase, it is important to characterize, at least partially, its boundary phases and phase coexistence regions. In the present work we did not investigate in detail the phase transitions between the different phases identified in the phase diagram. We will generically name

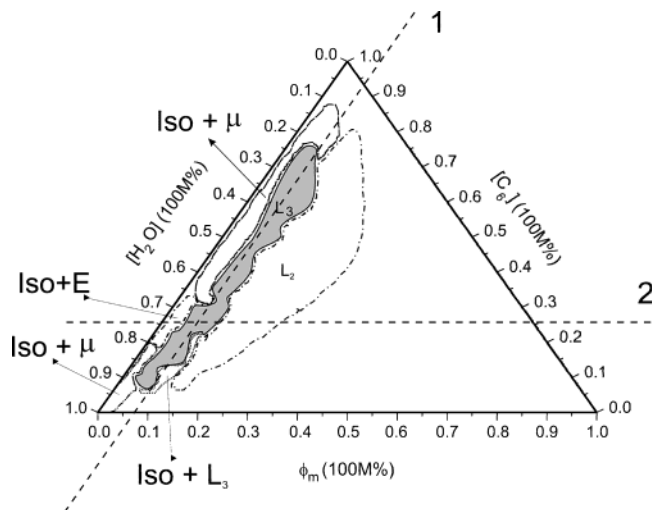


**Figure 1.** Partial isothermal ( $T = 21.5\text{ }^{\circ}\text{C}$ ) surface of the phase diagram of sodium dodecyl sulfate (SDS), cyclohexane ( $\text{C}_6$ ), 1-pentanol ( $\text{C}_5$ ), and water mixture, at  $[\text{SDS}]/[\text{C}_5] \approx 0.17$ , where  $[\ ]$  stands for mole percent ( $=M\%$ ). Line 1 and line 2 represent the loci of  $[\text{SDS} + \text{C}_5]$  and  $[\text{C}_6]$  about 7.5% and 25.4%, respectively.

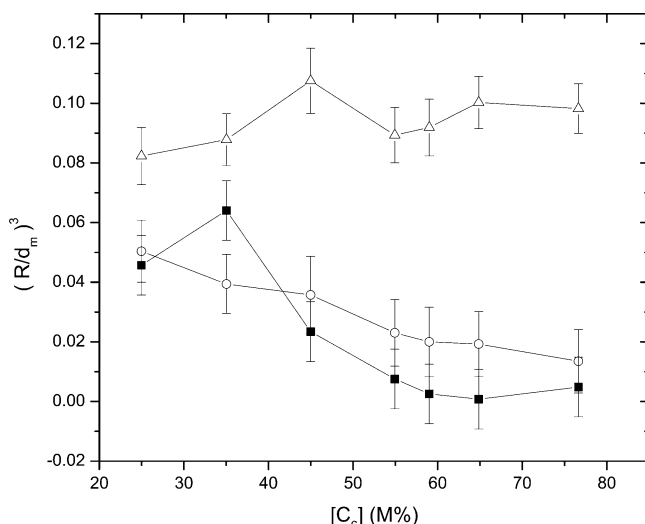


**Figure 2.** Parameter  $(R/d_m)^3$  as a function of  $[\text{C}_6]$  in the micellar isotropic phase.  $R$  is the radius of a spherical micelle, calculated from the Guinier radius of gyration, and  $d_m$  is the mean distance between them. ■, experimental results from X-ray scattering and diffraction experiments,  $\text{L}_2$  phase; ○, calculated values assuming inverted micelles in a bcc lattice; △, calculated values assuming direct micelles in a bcc lattice.  $\text{C}_6$  concentration range  $20\% < [\text{C}_6] < 75\%$  and  $\phi_m = 15\%$ . Solid lines are only guides for the eyes.

ISO an isotropic micellar phase not identified as  $\text{L}_1$  (made of direct micelles in a water-continuous medium) or  $\text{L}_2$  (made of inverse micelles in an oil-continuous medium) present in coexistence regions. At the left side of the  $\text{L}_3$  phase domain (i.e., at smaller values of  $\phi_m$ ) different coexistence regions were identified: in the ranges  $10\% \lesssim [\text{H}_2\text{O}] \lesssim 65\%$  and  $80\% \lesssim [\text{H}_2\text{O}] \lesssim 97\%$ , a coexistence between the ISO and microemulsion phase ( $\text{ISO} + \mu$  in Figure 1); in the range  $65\% \lesssim [\text{H}_2\text{O}] \lesssim 80\%$ , a coexistence between ISO and emulsion, this last one being thermodynamically unstable ( $\text{ISO} + \text{E}$  in Figure 1). In the right side of the  $\text{L}_3$  domain (i.e., at increasing values of  $\phi_m$ ), at  $70\% \lesssim [\text{H}_2\text{O}] \lesssim 90\%$  there is an almost linear coexistence region ( $\text{ISO} + \text{L}_3$ ). In contrast to the usual case of the phase diagrams where the direct sponge is present, a lamellar phase region was not observed in the phase diagram of Figure 1.

**Micellar Isotropic Phase Domain.** With increasing  $\phi_m$ , there is a large neighboring micellar isotropic phase domain. Considering that this domain spreads from  $[\text{H}_2\text{O}] \sim 10\%$  to  $[\text{H}_2\text{O}] \sim 90\%$ , one expects that both, direct and inverted, micellar isotropic phases are present. To investigate this aspect, we measured the Guinier radius of gyration of the micelles ( $R_g$ ) at  $\phi_m = 15\%$  by using the SAXS technique, and the mean distance between micelles ( $d_m$ ) by using X-ray diffraction technique, in the  $\text{C}_6$  concentration range  $20\% < [\text{C}_6] < 75\%$ . Figure 2 shows the ratio  $(R/d_m)^3$  as a function of the  $\text{C}_6$  concentration, where  $R = \sqrt{5/3}R_g$  is the radius of a spherical micelle. At this point, to check if this behavior is typical of a direct or inverted micellar phase, we assume a bcc lattice for the micellar system. Micelles are assumed to be spheres, and in this approximation, there are two micelles per unit cell. We verified that with the use of a different packing model, e.g., the hcp lattice, the results do not significantly differ from those presented here with the bcc lattice. In particular, the behavior of  $(R/d_m)^3$  as a function of  $[\text{C}_6]$  is qualitatively the same in both lattices. Knowing the mass ( $m_i$ ) and mass density ( $\rho_i$ ) of each component in a given mixture, the parameter  $(R/d_m)^3$  can be straightforwardly calculated in the framework of this model without any fitting parameter. In the case of inverted micelles

$$\left(\frac{R}{d_m}\right)^3 = \frac{3}{8\pi} \left( \frac{\rho_a}{\delta_a} - \frac{v_c}{V} \right) \quad (1)$$

with

$$\rho_a = \frac{\sum_{i=1}^4 m_i}{V} \quad \text{and} \quad \delta_a = \frac{\sum_{i=1}^4 m_i}{\sum_{i=1}^4 v_i}$$

where  $V$  is the total volume of the mixture;  $v_i = m_i/\rho_i$  and  $v_c$  represents  $v_i$  of  $\text{C}_6$ . In the case of direct micelles,  $v_c$  is replaced by  $v_w$  of water in eq 1. The values of the mass densities (in kilograms per liter) of  $\text{C}_6$ ,  $\text{C}_5$ , and SDS used are 0.78, 0.811, and 1.01, respectively.

The values of  $(R/d_m)^3$  as a function of  $[\text{C}_6]$ , for the direct and inverted micelles, are plotted in Figure 2. The error bars take into account the accuracy in the weighting processes of the different mixture components. Inspection of these results, particularly the behavior of  $(R/d_m)^3$  as a function of  $[\text{C}_6]$ , shows that (i) in the case of a direct structure,  $(R/d_m)^3$  tends to increase as  $[\text{C}_6]$  increases, and (ii) in the case of an inverted structure,  $(R/d_m)^3$  tends to decrease as  $[\text{C}_6]$  increases. In this framework, our experimental results indicate that the micellar isotropic phase in the  $[\text{C}_6]$  range studied is of the inverted type ( $\text{L}_2$ ). This conclusion is supported by electric ac conductivity and viscosity (Figure 3) measurements performed along the line  $\phi_m = 15\%$ . The monotonic behavior of the electric specific conductivity and viscosity in the concentration range  $20\% < [\text{C}_6] < 75\%$  does not put in evidence any drastic modification of the micellar structure in the micellar isotropic phase domain investigated.

**B. Dynamically Induced Birefringence.** All the samples present in the sponge phase domain of the partial isothermal investigated show a shear-induced birefringence. Figure 4 shows a typical curve of the normalized light transmittance, as a function of time, of a sponge phase sample with  $\phi_m = 7.5\%$  and  $[\text{C}_6] = 25.69\%$ , during the shear-induced birefringence experiment. The laser beam probes the velocity gradient induced by the falling of a stainless steel plate positioned inside the

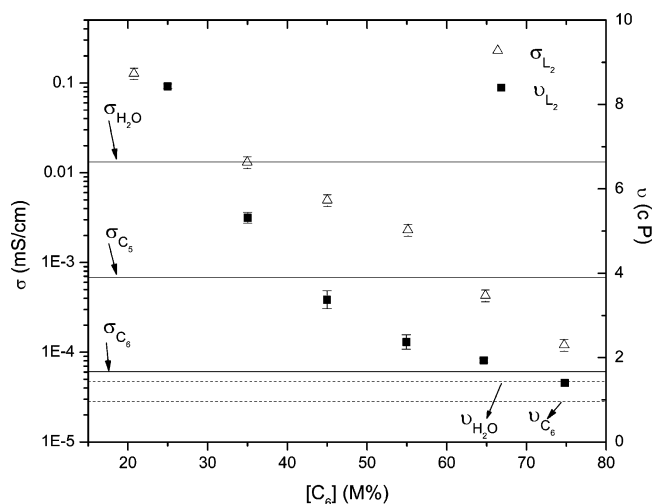


**Figure 3.** Electric ac specific conductivity ( $\sigma$ ) and viscosity ( $\nu$ ) as a function of  $[C_6]$  in L<sub>2</sub> phase.  $C_6$  concentration range 20%  $< [C_6] < 75\%$  and  $\phi_m = 15\%$ . Solid lines represent the specific conductivities of  $C_6$ ,  $C_5$ , and  $H_2O$ ; dashed lines represent the viscosities of water and  $C_6$ .

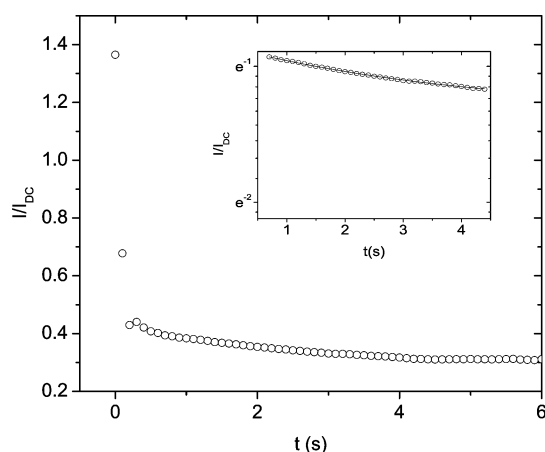


**Figure 4.** Normalized optical transmittance measured as a function of time in the shear-induced birefringence experiment. At  $t = 0$  the plate starts to impose the velocity gradient in the L<sub>3</sub> sample. The mixture concentrations are  $[SDS + C_5] = 7.5\%$  and  $[C_6] = 25.69\%$ . In the insert, a semilogarithmic plot of  $I/I_{DC}$  versus  $t$  and an exponential fit (solid line) are shown.

sample holder. At  $t = 0$  the plate starts to impose the velocity gradient in the sample, which is maintained during the time of falling of the plate. At  $t \sim 0.4$  s the plate movement stops, and at  $t \approx 4.6$  s the induced birefringence vanishes. An exponential fitting curve with characteristic time  $\tau = 3.2$  s is shown in the insert of Figure 4, in the range  $0.5 \text{ s} \leq t \leq 4.5$  s. After the movement of the plate stops, the birefringence vanishes with a relaxation time  $\tau$ . This relaxation time is 2 orders of magnitude larger than that of the induced birefringence (by using the same experimental setup) in an isotropic micellar phase of the potassium laurate, 1-decanol, and water mixture.<sup>20</sup>

**C. Polarized Optical Microscopy.** As discussed in the Introduction, the L<sub>3</sub> phase is optically isotropic. However, some of the samples in the sponge phase domain investigated presented small birefringent regions when they are conditioned in flat glass capillaries  $\lesssim 50 \mu\text{m}$  thick. These birefringent regions are less than 20% of the total area of the sample, and the rest of the sample is optically isotropic. It is important to stress that this result was *not observed* in thick samples.

The presence of these birefringent regions is puzzling. Dvolaitzky and co-workers<sup>14</sup> reported the existence of what they

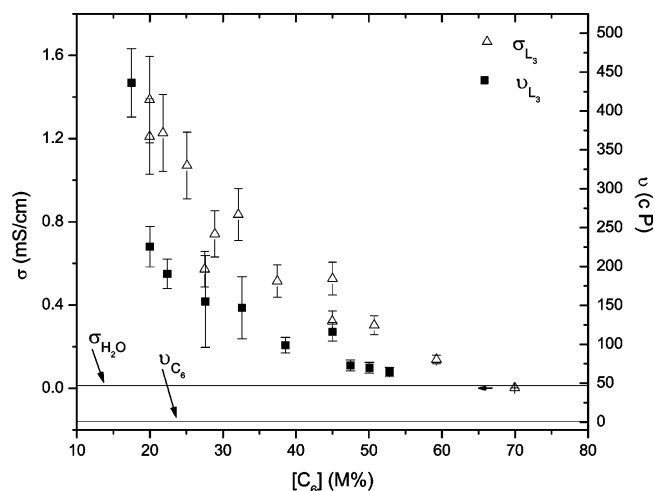


**Figure 5.** Viscosity ( $\nu$ ) and electric ac specific conductivity ( $\sigma$ ), at 1 kHz, of sponge phase samples as a function of  $[C_6]$  (along line 1). Solid lines represent the viscosity of  $C_6$ , which is 0.992 cP, and the measured electric ac specific conductivity of water.

called “birefringent microemulsions” in the bulk of some samples of the same quaternary mixture we investigate in this work. One of their samples, presenting this characteristic, is (approximately) placed in the partial isothermal phase diagram of Figure 1, at  $[C_6] \sim 40\%$  and  $[H_2O] \sim 50\%$ . NMR, neutron scattering, and X-ray scattering results suggested that this type of phase could be constituted by a dispersion of big anisotropic molecular aggregates (10 nm large) that, as a function of time, self-assemble in bigger anisotropic structures. These structures should be very sensitive to velocity gradients mechanically imposed on the sample, which could break these bigger aggregates. In our case, however, we did not observe this particular behavior in the bulk of all the samples investigated.

A possible origin of the birefringent regions observed by us in sponge phase samples placed in thin cells could be due to the wetting phenomenon of the sample holder’s surfaces. In a previous work<sup>19</sup> we reported on the effect of what we called “the surface field” in the sample–glass interface, which could induce (at the interface) a phase transition to an anisotropic phase. A selective adsorption of amphiphilic molecules by the glass surfaces imposes a concentration gradient at the interface, which drives the phase transition from the L<sub>3</sub> to an anisotropic phase structure. A possible phase that could be formed at the interface is the lamellar phase.<sup>19</sup> However, recent grazing X-ray diffraction results obtained with this lyotropic mixture wetting different substrates indicate the presence of an induced tetragonal structure in a thin layer at the sponge phase–substrate interface.<sup>15</sup>

**D. Viscosity Measurements.** Figure 5 shows the viscosity ( $\nu$ ) of the sponge phase samples as a function of the molar concentration of cyclohexane ( $17.5\% < [C_6] < 52.5\%$ ), along line 1, at  $\phi_m = 7.5\%$ . The viscosity decreases as  $[C_6]$  increases, and its value tends asymptotically toward  $\nu \sim 60$  cP at  $[C_6] \geq 50\%$ . This value is about 1 order of magnitude larger than those of both solvents present in the mixture (the viscosities of  $C_6$  and water at  $T \sim 24^\circ\text{C}$  are 0.992 and 1.102 cP, respectively). Even in mixtures with the highest water concentration ( $[C_6] \sim 17.5\%$ ), the viscosity measured is 2 orders of magnitude higher than that of pure water. These results give us interesting hints about the structure of the sponge phase in the bulk. The monotonic decreasing of the sample viscosity as  $[C_6]$  increases seems to indicate that no drastic modifications of the structure (e.g., from direct to inverted) are expected along all the sponge phase domain investigated.



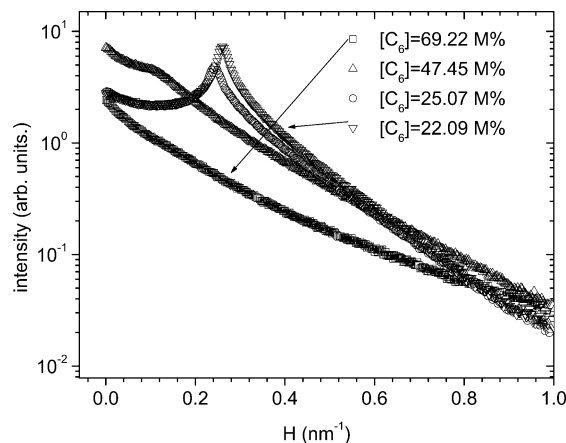


**Figure 6.** Small-angle X-ray scattering curves (semilogarithmic plot) of sponge phase samples with different  $[C_6]$ , along line 1 of the partial isothermal surface of the phase diagram.

**E. Electric ac Conductivity Measurements.** The electric ac specific conductivity ( $\sigma$ ) measurements (Figure 5) along line 1 ( $20\% < [C_6] < 70\%$ ) also show a monotonically decreasing behavior as a function of increasing  $[C_6]$ . At  $[C_6] > 70\%$  the ac specific conductivity tends asymptotically to its value at the isotropic micellar (expected inverted) phase, which is  $(1.3 \pm 0.2) \times 10^{-2}$  mS/cm. This value is of the same order of magnitude as the ac specific conductivity of water and is much larger than the ac specific conductivity of  $C_6$  (at  $T \sim 24^\circ\text{C}$ ), which are  $1.304 \times 10^{-2}$  and  $6.06 \times 10^{-5}$  mS/cm, respectively, measured in the same setup. Despite the large interval of variation of  $[C_6]$  investigated, the monotonic behavior of the electric conductivity indicates that no drastic modification (as, for example, a transition from inverted to direct structure) of the local structure of the phase seems to take place. Obviously, the specific conductivity measurements alone do not lead to this conclusion about the phase structure, and complementary techniques are necessary to overcome this difficulty. This aspect will be discussed in the following.

**F. X-ray Diffraction Results.** A typical X-ray diffractogram of the sponge phase in high angles presents a broad band that corresponds, in the direct space, to the distance  $0.5 \pm 0.1$  nm. This value is associated with the mean distance between carbonic chains and is independent of  $[C_6]$ .

**G. Small-Angle X-ray Scattering.** The small-angle X-ray scattering curves of a representative set of  $L_3$  samples along line 1 (four samples) and line 2 (four samples) of the partial isothermal surface of the phase diagram (Figure 1) are shown in Figures 6 and 7, respectively. These results were obtained in the SAXS beam line of the LNLS synchrotron.

Let us first analyze the results along line 1, i.e., at a fixed  $\phi_m$ . A band is observed in small angles in the scattering curves of samples with a higher water concentration. The sample with  $[C_6] = 47.45\%$  presents a “shoulder” in the SAXS curve, and the sample with  $[C_6] = 69.22\%$  does not show the band. The band becomes more defined, narrow and intense, and its position, in the reciprocal space, moves to large values of  $H$  as the water concentration increases. Mixtures with  $[C_6] \lesssim 25\%$  are those that present the more narrow bands. The characteristic distance ( $d$ ) associated with this band ranges (Figure 8) from 25 to 60 nm, with increasing  $[C_6]$ . We will associate  $d$  with the mean distance between  $C_6$  channels of an *inverted sponge structure*. From the width at half-height of the band, the correlation distance ( $D$ ) was calculated as being on the order of 45 nm (Figure 9), which is on the order of  $1.5d$ . The region of the SAXS curves where  $H \rightarrow 0$  (far ahead the band or

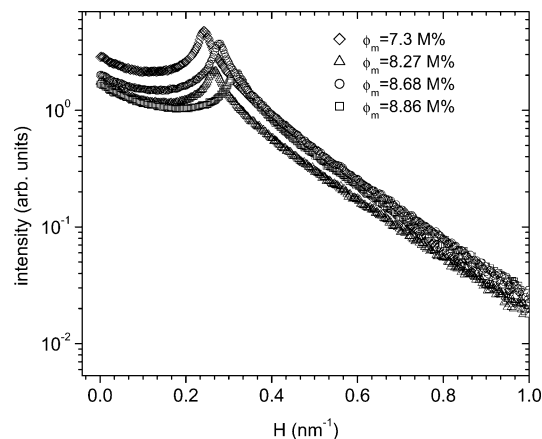


**Figure 7.** Small-angle X-ray scattering curves (semilogarithmic plot) of sponge phase samples with different  $[SDS + C_5]$ , along line 2 of the partial isothermal surface of the phase diagram.

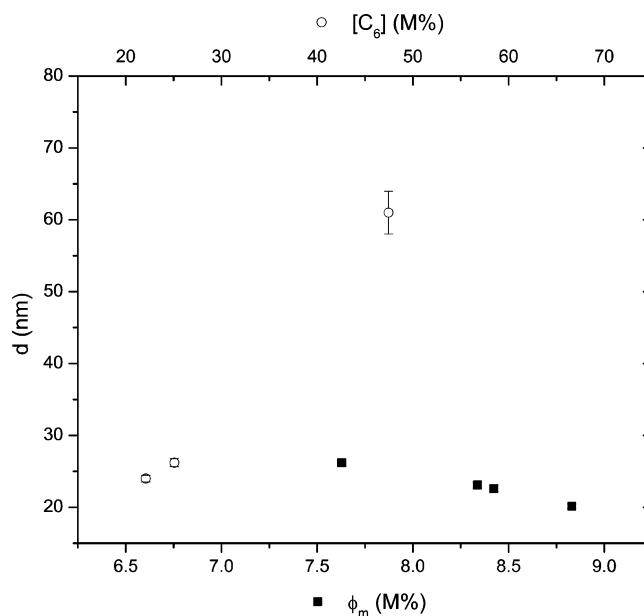


**Figure 8.** Average distance  $d$  associated with the band present in the SAXS curves of a set of representative samples: (○) along line 1; (■) along line 2.

shoulder position) can be used to evaluate the parameter  $\delta$ , associated with the lipid bilayer in direct sponge phases, or the thickness of the polar solvent layer in the case of inverted structures. Figure 10 shows a typical semilog plot of  $I(H)H^2 \times H^2$ , where  $I(H)$  is the measured scattering intensity of a sample along line 1. This plot allows the determination of the parameter  $\delta$  by means of the fit of a Guinier-type function:<sup>12</sup>  $I(H) \propto \exp(-\delta^2 H^2/12)$ . Figure 11 shows  $\delta$  as a function of  $[C_6]$  along line 1.  $\delta$  shows a decreasing behavior when  $[C_6]$  increases, indicating that the structure is of the inverted type in the concentration range investigated. In this picture,  $\delta$  represents the water layer that separates two nonconnected regions of cyclohexane. Our results, at the present stage, do not allow us to determine other characteristic parameters of the structure, such as the area occupied by the polar head ( $S_p$ ) at the interface. However, let us discuss, at least qualitatively, the expected behavior of this parameter in the  $[C_6]$  range investigated. Gallot and Skoulios<sup>21</sup> measured  $S_p$  as a function of the ratio  $Z = [\text{water}]/[\text{Na soap}]$  in binary mixtures in the lamellar phase. They observed that  $\log(S_p) \approx 0.24 \log(Z)$ . In our case  $[C_6]$  increases from  $\sim 20\%$  to  $70\%$ , at a fixed  $\phi_m$ , the water concentration decreases from  $\sim 70\%$  to  $\sim 25\%$ , and consequently,  $Z$  decreases along this line

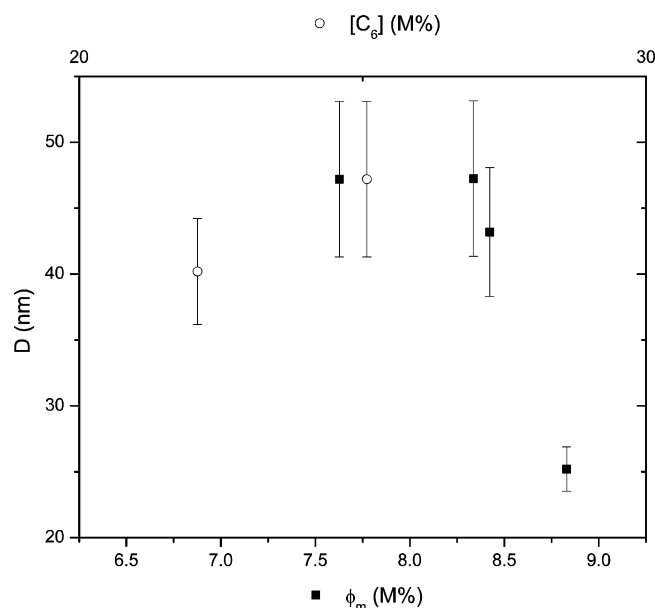


**Figure 9.** Correlation distance  $D$  obtained from the width at half-height of the bands present in the scattering curves: (○) along line 1; (■) along line 2.

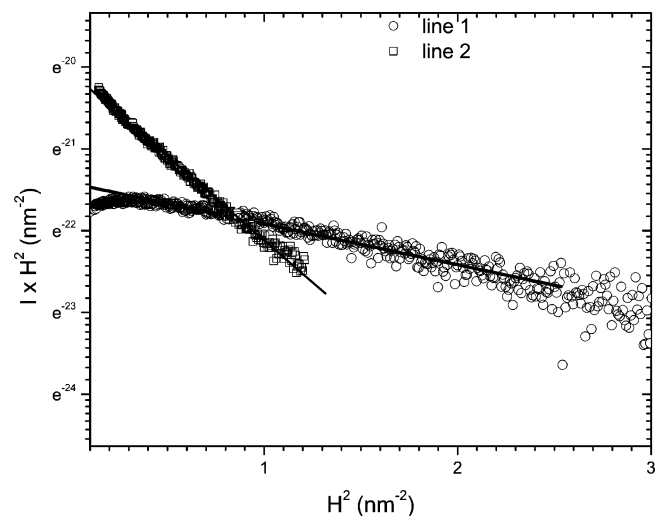


**Figure 10.** Semilogarithmic plot of  $I(H)H^2 \times H^2$ , where  $I(H)$  is the measured scattering intensity in the limit of  $H \rightarrow 0$ , of the scattering data of a typical sponge phase sample: (○) along line 1; (■) along line 2.

from  $\sim 4.7$  to  $\sim 1.7$ . Assuming that the amphiphiles of our mixture behave like the Na soap investigated by Gallot and Skoulios, one should expect that along this line, increasing the C<sub>6</sub> concentration,  $S_p$  decreases by a factor of  $\sim 1.3$ .

Along line 2, the SAXS curves of different samples (Figure 7) with varying  $\phi_m$  also present a band in small angles. The characteristic distance ( $d$ ) associated with this band (Figure 8) decreases from about 26 to 20 nm, with increasing  $\phi_m$ . The correlation distance ( $D$ ) is on the order of 45 nm (Figure 9) at  $\phi_m \lesssim 8.5\%$ , which is also on the order of  $2d$ . At higher  $\phi_m$  ( $\sim 8.8\%$ ), near the L<sub>3</sub>-to-L<sub>2</sub> phase transition,  $D \sim 25$  nm, indicating a loss of positional correlation as the mixture approaches the micellar isotropic phase. Figures 10 and 11 show a typical semilogarithmic plot of  $I(H)H^2 \times H^2$  and  $\delta$  as a function of  $\phi_m$ , respectively, along line 2.  $\delta$  shows a decreasing behavior when  $\phi_m$  increases. This result is consistent with the picture of an inverted-type structure, where  $\delta$  represents the water layer that separates two nonconnected regions of cyclohexane, in the concentration range of amphiphiles investigated.

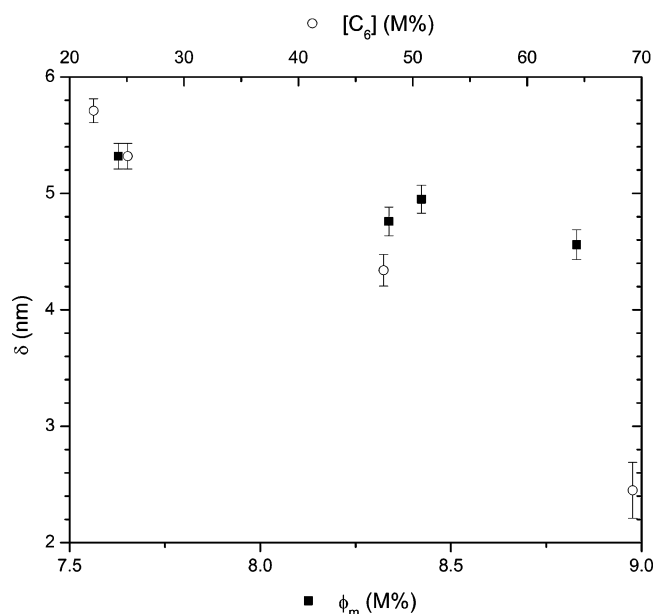


**Figure 11.** Water layer thickness  $\delta$ : (○) as a function of  $[C_6]$ , along line 1; (■) as a function of  $[SDS + C_5]$ , along line 2.

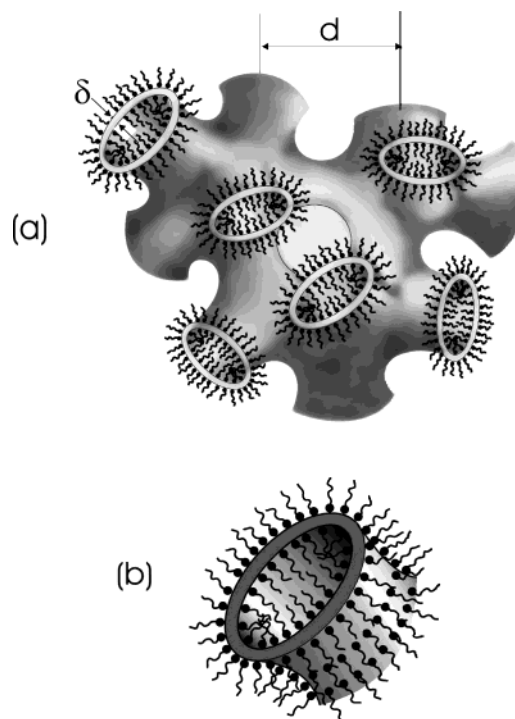


**Figure 12.** Sketch of the proposed inverted structure of the sponge phase in the partial isothermal surface of the phase diagram studied: (a) overall view; (b) detail of the water layer of thickness  $\delta$ .

At this point we can compare our scattering results with a typical one obtained by Strey and co-workers<sup>22</sup> in the direct sponge phase. They studied the C<sub>12</sub>E<sub>5</sub>/water mixture by using the small-angle neutron scattering technique and found, at  $\phi = 0.103\%$ ,  $d \sim 7$  nm and  $D \sim 11$  nm, which gives  $D/d \sim 1.6$ . In our case, along line 1,  $0.8 \lesssim D/d \lesssim 2.3$  and, along line 2,  $1.7 \lesssim D/d \lesssim 2.3$ , which are of the same order of magnitude as that measured in direct structures. The difference, however, is in the fact that our values of  $D$  and  $d$ , independently, are larger than those found in the direct sponge structures.

**H. Proposed Structure for the Sponge Phase.** The results accumulated from the different experimental techniques point to an *inverted structure* for the L<sub>3</sub> phase, in the concentration

range investigated, of the partial isothermal surface of the phase diagram of Figure 1. Figure 12 presents a sketch of this structure. In this structure, a water layer of thickness  $\delta$  separates two nonconnected regions with the  $C_6$ . This water layer is separated from the  $C_6$  by the polar heads of the SDS and OH groups from the  $C_5$  molecules. We identify the mean distance between the internal  $C_6$  channels in the inverted structure as the parameter  $d$  measured from the X-ray scattering and diffraction experiments.

Let us summarize the experimental results to show that they are consistent with the proposed picture for the  $L_3$  phase investigated:

1. The monotonic decreasing behavior of  $v$  as  $[C_6]$  increases (Figure 5) can be understood, observing that the distance between the  $C_6$  channels ( $d$ ) increases (Figure 8) as  $[C_6]$  increases. This "swelling" of the structure provides an unstiffness of it, reducing the sample viscosity.

2. The electric ac specific conductivity (Figure 5) also presents a monotonic decreasing behavior as  $[C_6]$  increases. Its value tends to that of the inverted  $L_2$  phase, where the structure is constituted by water globules (in contact with the polar heads of the SDS and the OH groups of the  $C_5$  molecules) surrounded by  $C_6$ . The electric ac specific conductivity behavior in this  $L_2$  phase is essentially determined (dominated) by the water globules in the continuous  $C_6$  medium. The monotonic decreasing of  $\sigma$  in the sponge phase domain, line 1, without any discontinuity (that should be expected if an inverted-to-direct transition occurred along this line) is consistent with the picture of inverted structure for the sponge phase studied. The bigger the  $C_6$  concentration, the larger the  $C_6$  nonconnected domains separated by the water layer, and the more the sample specific conductivity behaves like that of the  $L_2$  phase, with water globules in a continuous  $C_6$  medium.

3. The behaviors of  $d$  (associated with the distance between  $C_6$  channels) and  $\delta$  (associated with the water layer that separates the two nonconnected  $C_6$  regions), as a function of  $[C_6]$  (line 1) and  $[SDS + C_5]$  (line 2), Figures 8 and 11, are consistent with the inverted sponge structure in the partial isothermal investigated: (i) as  $[C_6]$  increases  $d$  increases and  $\delta$  decreases; (ii) as  $[SDS + C_5]$  increases  $d$  and  $\delta$  decreases.

**Acknowledgment.** We are greatly indebted to Prof. I. Torriani, Dr. S. Kycia, Dr. G. Kellerman, Mr. J. V. de Oliveira Neto, and Mr. T. Plivelic from the Laboratório Nacional de Luz Sincrotron (LNLS), Campinas, São Paulo, Dr. R. Itri, Mr. E. L. Duarte, and R. T. dos Santos from IFUSP. The FAPESP, CNPq, and PRONEX are acknowledged for financial support.

## References and Notes

- (1) Roux, D.; Cates, M. E.; Olsson, U.; Ball, R. C.; Nallet, F.; Bellocq, A. M. *Europhys. Lett.* **1990**, *11*, 229.
- (2) Alfons, K.; Engstrom, S. *J. Pharm. Sci.* **1998**, *87*, 1527.
- (3) Drummond, C.; Fong, C. *Curr. Opin. Colloid Interface Sci.* **2000**, *4*, 449.
- (4) Talmon, Y.; Prager, S. *J. Chem. Phys.* **1978**, *69*, 2984.
- (5) Porte, G.; Appell, J.; Bassereau, P.; Marignan, J. *J. Phys. Fr.* **1989**, *50*, 1335.
- (6) Balinov, B.; Olsson, U.; Söderman, O. *J. Phys. Chem.* **1991**, *95*, 5931.
- (7) Magalhães, M.; Pusioli, D.; Ramia, M. E.; Figueiredo Neto, A. M. *J. Chem. Phys.* **1998**, *108*, 3835.
- (8) Gazeau, D.; Bellocq, A. M.; Roux, D.; Zemb, T. *Europhys. Lett.* **1989**, *9*, 447.
- (9) Maldonado, A.; Urbach, W.; Ober, R.; Langevin, D. *Phys. Rev. E* **1996**, *54*, 1774.
- (10) Porte, G.; Delsanti, M.; Billard, I.; Skouri, M.; Appell, J.; Marignan, J.; Debeauvais, F. *J. Phys. II Fr.* **1991**, *1*, 1101.
- (11) Skouri, M.; Marignan, J.; Appell, J.; Porte, G. *J. Phys. II Fr.* **1991**, *1*, 1121.
- (12) Filali, M.; Appell, J.; Porte, G. *J. Phys. II Fr.* **1995**, *5*, 657.
- (13) Porte, G.; Marignan, J.; Bassereau, P.; May, R. *J. Phys. Fr.* **1988**, *49*, 511.
- (14) Devolaitzky, M.; Ober, R.; Billard, J.; Taupin, C.; Charvolin, J.; Hendricks, Y. C. *R. Acad. Sci. Paris* **1981**, *292*, 45.
- (15) Magalhães, M.; Figueiredo Neto, A. M.; Barbero, G.; Tromba, A. C. *J. Phys. Chem. B* **2003**, *107*, 13949.
- (16) Fabre, P.; Casagrande, C.; Veyssie, M.; Cabuil, V.; Massart, R. *Phys. Rev. Lett.* **1990**, *64*, 539.
- (17) Quilliet, C.; Fabre, P.; Cabuil, V. *Phys. Chem.* **1993**, *97*, 287.
- (18) Ponsinet, V.; Fabre, P. *J. Phys. Chem.* **1996**, *100*, 5035.
- (19) Magalhães, M.; Figueiredo Neto, A. M.; Tolédano, P. *Phys. Rev. E* **2000**, *62*, 5847.
- (20) Fernandes, P. R. G.; Figueiredo Neto, A. M. *Phys. Rev. E* **1995**, *51*, 567.
- (21) Gallot, B.; Skoulios, A. E. *Kolloid-Z.* **1968**, *208*, 37.
- (22) Strey, R.; Schomacker, R.; Roux, D.; Nallet, F.; Olsson, U. *J. Chem. Soc., Faraday Trans.* **1990**, *86*, 2253.